

PAPER • OPEN ACCESS

Stability Study of Anthropomorphic Robot Antares under External Load Action

To cite this article: A S Kodyakov *et al* 2017 *J. Phys.: Conf. Ser.* **803** 012074

View the [article online](#) for updates and enhancements.

You may also like

- [ANTARES and IceCube Combined Search for Neutrino Point-like and Extended Sources in the Southern Sky](#)
A. Albert, M. André, M. Anghinolfi et al.
- [Constraining the neutrino emission of gravitationally lensed Flat-Spectrum Radio Quasars with ANTARES data](#)
S. Adrián-Martínez, A. Albert, M. André et al.
- [ANTARES Search for Point Sources of Neutrinos Using Astrophysical Catalogs: A Likelihood Analysis](#)
A. Albert, M. André, M. Anghinolfi et al.



The Electrochemical Society
Advancing solid state & electrochemical science & technology

242nd ECS Meeting

Oct 9 – 13, 2022 • Atlanta, GA, US

Presenting more than 2,400
technical abstracts in 50 symposia



ECS Plenary Lecture
featuring
M. Stanley Whittingham,
Binghamton University
Nobel Laureate –
2019 Nobel Prize in Chemistry



Register now!



Stability Study of Anthropomorphic Robot Antares under External Load Action

A S Kodyakov¹, N A Pavlyuk¹, V Yu Budkov¹, R A Prakupovich²

¹ St. Petersburg Institute for Informatics and Automation of the Russian Academy of Sciences, St. Petersburg, Russia

² United Institute of Informatics Problems, Minsk, Belarus

E-mail: ronzhin@ias.spb.su

Abstract. The paper presents the study of the behavior of the major structural elements of the lower limbs of anthropomorphic robot Antares under the influence of different types of loads (torsion, fracture). We have determined the required values for actuators torques for motion of the robot in space. The maximum values of torques are 5 Nm and 5.2 Nm respectively, and are able to withstand the upper and lower leg structures.

1. Introduction

Modern developments in the field of humanoid robotics are aimed at making motion characteristics of the robot closer to the kinematics of the human body [1,2]. The problem of high energy consumption in the realization of the kinematics of the anthropomorphic robot is partially solved by making the construction lighter. Auxiliary batteries (an installation site is provided) will be installed in the upper legs to reduce the electrical load on the main battery of Antares as well as to control actuator powering, which will help to avoid power supply problems. In this regard, the study of the stability of structures and materials and their ability to withstand a given load is of particular interest [3,4].

One of the simplest structures of the biped robot is described in [5]. It is made up of a two-millimeter aluminum sheet, includes six servos operated by an EyeBot controller, and weighs 1.11 kg. When walking, the robot reaches a speed of 120 m/h at a maximum angle of 60 degrees between the hips. Such robot architecture with six servos is used in [6] to study the operating angles of the joints of the knee, ankle and hip.

The anthropomorphic robot in the HanSaRam series, which regularly participates in the FIRA league since 2000, is discussed in [7]. The HanSaRam-VIII (HSR-VIII) robot has 28 servos, weighs 5.5 kg and can move at a speed of up to 12 cm/s.

In [8], anthropomorphic robot Lola, having 7 degrees of freedom per leg, weighs 55 kg with the 180 cm height. The problems of stability of the robot after stopping as well as a gradual contact of foot parts with the surface when walking are discussed. Elastic materials of the toe and heel of the robot foot ensure the reduction of impact force on the robot structure during touching the surface.

A home assistive robot with 14 servos and 16 degrees of freedom, presented in [9], has an anthropomorphic upper body architecture and a wheelbase. The paper mostly focuses on two-handed manipulation of objects by robots during transferring domestic objects.

Anthropomorphic robot SWUMANOID, 92 cm high, having 24 servomechanisms of the series Dynamixel in its construction, is designed in [10] to simulate motions and swimming in water.



Unstable rolling of the robotic body in water complicates the calculation of the kinematics of movements of a floating robot that consists of 21 composite components.

After reviewing the humanoid robot structures [11, 12] and focusing on the literature [13, 14], we have developed a model of robot Antares (Fig. 1). Antares is a robotic system designed for research activities. Its construction, as that of robot DARwin OP [12], consists of parts made from Duralumin D16T plates (2, 4, 8, 12 mm thick). The developed model of Antares has a number of advantages compared with robot Poppy [11]. These include an increased operating range of motors installed in the legs; the use of a more durable material; more optimal distribution of the internal space of the robot.

Details of anthropomorphic robot Poppy are created based on 3D-printing, which allowed much cheaper production of the robot parts and made it possible to use less powerful servos, but reflected on robot stability when walking. The robot has 25 servomechanisms Dynamixel MX-64 and MX-28 [12], which ensure unobstructed movement of the limbs with a given accuracy and strength margin as gears are made of metal.

A modular robot design helps the researcher to change the movement of any robot's limb by isolating the desired limb from the rest of the body, almost without affecting the performance. The structure is specially designed for the installation of additional sensors and connection cables. In addition, such a design facilitates periodic robot maintenance service.

Robot Darwin-OP is a robot platform intended for research and development within the framework of an educational process. DARwin OP has high performance and dynamic characteristics and a wide range of sensors.

A modular robot design helps the researcher to change the movement of any limb of DARwin OP. The structure also allows the installation of additional sensors.

In this paper, we study the stability of the basic structural elements of anthropomorphic robot Antares (Fig. 1) when subjected to external forces such as linear force and torsion. During the research, we have analyzed the movement of the lower limbs and modelled the impact of the external load on the constituent elements of robot's structure. Due to the use of lightweight materials, the engines consume less energy. Dynamixel actuators MX-64T (engines Nos. 1-12) and MX-28 (engines Nos. 13-22) are used in the construction of Antares; the gears are made of metal, which ensures movements with a given accuracy and a margin of safety [12].

The modular construction of the robot allows the researcher to change the movement of any robot's limb by isolating the desired limb from the rest of the body almost without affecting the performance. The structure allows for the installation of additional sensors and connection cables. Furthermore, such a design facilitates periodic maintenance service for the robot. The estimated height of the robot is 100 cm and the weight is 6 kg.

2. Motion analysis of lower limbs

Motion analysis is regarded as the movement of a three-dimensional model in the conditions close to real ones and the reading from sensors. The model of the robot, shown in Fig. 1, displays numbering of servomotors, for which the motion analysis is carried out using the method proposed in [15,16]. The purpose of the simulation is to determine the values of the torque and linear force acting on the robot structure. Data from the obtained results can be used to simulate weight loads on various positions of the robot in space. In the simulation process, we have determined the torques of the engine output shaft in the joints of robot's leg (ankle, knee and pelvis joints).

To analyze the motion, robot's foot was blocked while the leg was moving. Force of gravity G equals 9.81 m/s^2 . The contact between the motor flanges and upper and lower leg plates was simulated. Then, equal parameters were set for four engines Nos. 2-5 (Fig.2). In the engine parameters, the function "segments" was selected, where engine's running time is 3 seconds; the motor shaft is moving at 85° ; the type of segment is cubic. We used the force that replaced the weight of robot's torso of 20 N as the external load. To determine the torque on the engine shafts Nos. 2-5 (Fig. 2), sensors were installed. The engines worked synchronously and their running time was 3 seconds.

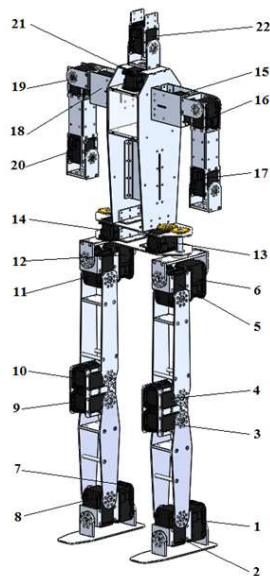


Figure 1. Engines of the generalized model of anthropomorphic robot Antares

As we can see clearly from the graphs, shown in Fig. 2, the engines need different torques to raise the torso. Engine No.2 only maintains balance, so it has a small torque in comparison with engine No. 3. The latter, rotating in the knee joint, moves the lower leg (which abuts against the foot), thus elevating the leg. The situation is similar with engines No. 4 and No. 5. Engine No. 4 lifts robot's leg, abutting against engine No. 3, while engine No. 5 maintains balance.

For engine No. 2, the torque is $\tau = 0.3 \text{ N}\cdot\text{m}$, and for engine No. 3 the torque is $\tau = 4.5 \text{ N}\cdot\text{m}$, so the total torque in the initial period of time approximately equals $0.3 + 4.5 = 4.8 \text{ N}\cdot\text{m}$. The torque per one engine is $2.4 \text{ N}\cdot\text{m}$. The moment of force applied to the assembly of the lower leg when robot's leg is in a "sitting position" is as follows:

$$F = \frac{\tau}{l} = \frac{2,4}{0.17} = 14,11 \approx 15 \text{ N},$$

where l is the length of the arm on which the force is acting.

For engine No. 4 the torque is $\tau = 4.5 \text{ N}\cdot\text{m}$, and for engine No. 5 the torque is $\tau = 0.5 \text{ N}\cdot\text{m}$, therefore, the total torque in the initial period of time is equal to $4.5 + 0.5 = 5 \text{ N}\cdot\text{m}$. The torque per one engine is $2.5 \text{ N}\cdot\text{m}$.

The moment of force applied to the upper leg when robot's leg is in a "sitting position" is equal to:

$$F = \frac{\tau}{l} = \frac{2,5}{0.17} = 14,7 \approx 15 \text{ N}.$$

Thus, based on the motion analysis of two leg assemblies, we determined moments that act on the parts of leg when lifting it from the "sitting position". These moments served to model the application of external loads to the assemblies of the lower and upper leg.

3. Simulation of weight loads on the lower limbs of Antares

Load modeling is testing if robotic parts and joints can withstand different loads as well as identifying weak spots in the structure. The essence of conducting the analysis of structural assemblies is to see what stresses occur in robot's details. On the basis of this analysis, we can evaluate if the developed model of the robot is suitable for carrying out different tasks.

We have studied the assembly of the upper and lower leg. The material selected was duralumin alloy D16T and brass. Duralumin was used for making plates for a lower and upper leg and a transverse strut. Brass was used for making a stiffening rib for an upper and lower leg. Duralumin is destroyed at a lower load than brass is [15], so the simulation process is terminated after reaching the threshold of destruction of duralumin. The "global contact (no movement)" was selected as the type of

attachment. Surfaces of working holes served as a place of attachment. In addition to the “global contact”, we have used a type of the connection “bolt-connector” for even load distribution. The assemblies are fixed with the help of “fixed geometry” which does not allow feet assemblies to move in servo flanges’ attaching point. The linear force and torque were used as the external load at fixing points of servo flanges. Estimated weight of the robot assembly is 6 kg, with each leg weighing about 1 kg. Half the weight of robot’s body (excluding legs) accounts for the assembly of one leg, which is approximately 20 N. This value was calculated for the vertical and lateral (along the normal to the front plane) load according to the following formula:

$$F = P/2 = 40/2 = 20 \text{ N,}$$

where F is the force applied to the lower leg assembly; P is weight of legs; the denominator is 2, since all weight is distributed over 2 legs.

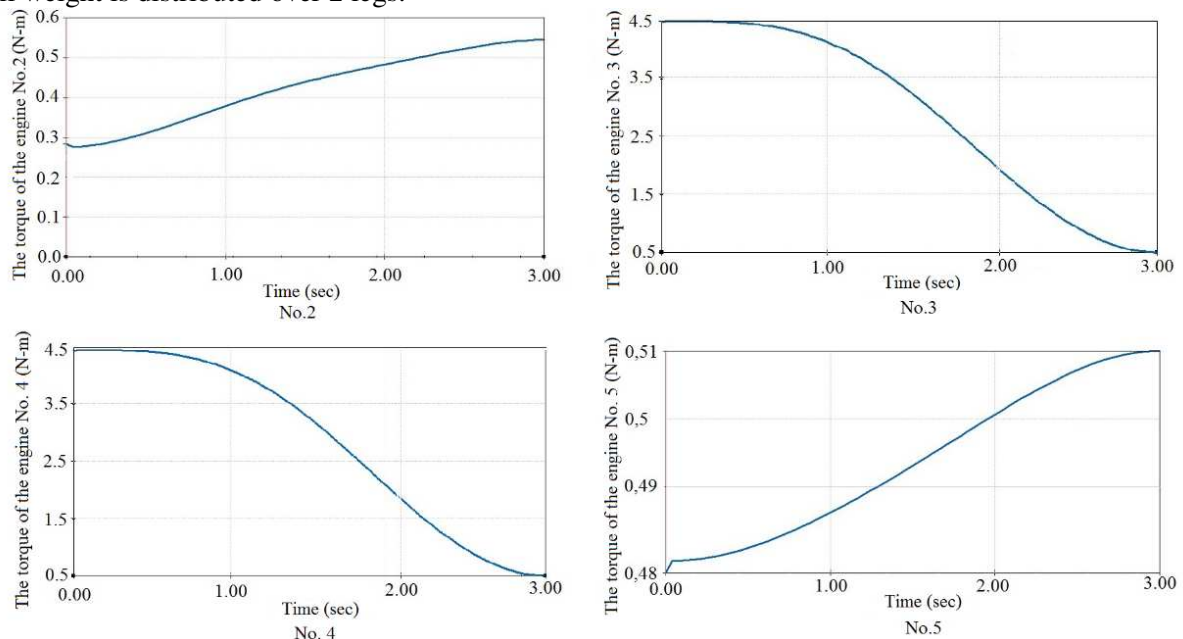


Figure 2. Dependence of torques of engines Nos. 2-5 on their running time for the leg construction

During the simulation process, assemblies were exposed to 2 types of loads - torque and linear force aimed at three directions: vertical (perpendicular to the transverse plane), lateral (along the normal to the front plane) and lateral (perpendicular to the sagittal plane).

Vertical load and lateral load (sitting position) on the assembly of the lower leg (or upper leg) accounts for 25 H, as 20 H is torso’s weight and 5 H is the weight of the upper leg; only torso’s weight (20 H) accounts for the upper leg.

For lateral load (position of the legs in cross splits), the force value was calculated based on the leg “motion analysis”. It is equal to 20 H, since 15 H is torso’s weight, and 5 H is the weight of the upper leg; only torso’s weight (15 H) accounts for the upper leg.

Since motor’s torque varies from 0 to 6 N·m, the simulation was carried out for the maximum torque value with the application of external vertical and lateral loads. The direction of the applied force is selected based on the fact that this force will have its maximum value when the foot is in the “sitting” position. Therefore, the direction will be along the normal to the sagittal plane of the leg.

To test the leg for torsion, we have modeled such a scenario when the robot is in a prone position and the inner part of its feet rests against the floor surface. Torsion occurs throughout the whole length of the leg (0.5 m), therefore, the torque is the same for the assemblies of the lower and upper leg. For the assembly of the leg (with the foot length equal to 0.0825 m and the weight of the leg - 1 kg), the torque has the following value:

$$\tau = F \cdot l = 10 \cdot 0,0825 = 0,825 \text{ N} \cdot \text{m.}$$

Figures 3 and 4 present the results of load modelling in the form of stress distribution diagrams, on the basis of which it is possible to draw conclusions about the behavior of the upper and lower legs assemblies under different kinds of applied load. The diagram of internal stresses reflects the ability of a part or assembly to withstand the applied loads.

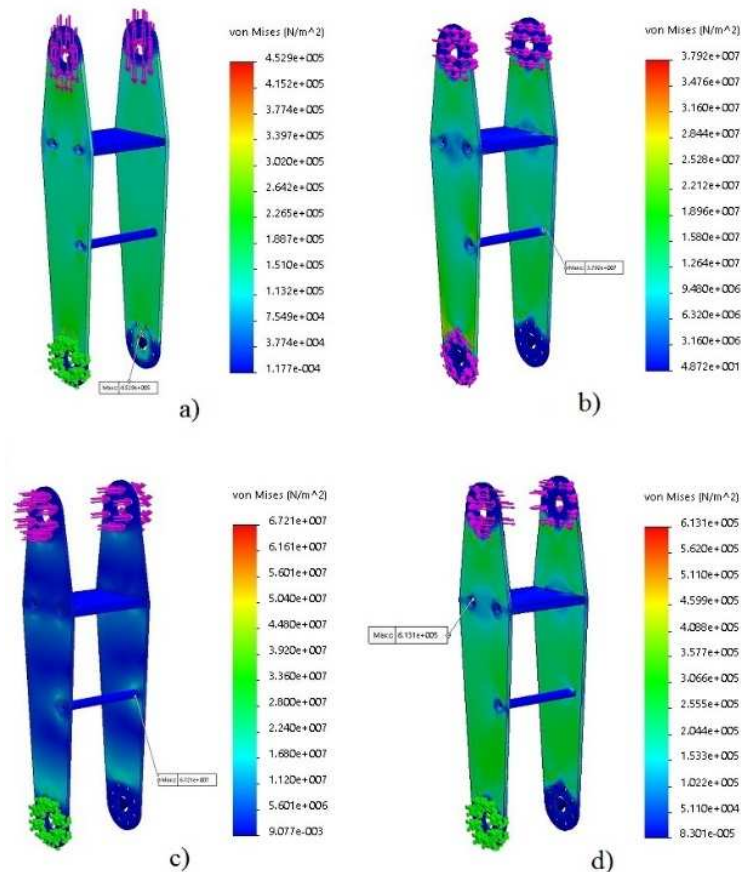


Figure 3. The simulation results of the lower leg model: a) vertical load; b) torque load and lateral load (along the normal to the transverse plane); c) lateral load (perpendicular to the sagittal plane); d) torsion

Diagrams of the maximum internal stresses are built according to von Mises and evaluated according to equivalent internal stresses in comparison with the yield strength of the used material. The material used for making the product begins to weaken when the stress according to von Mises is equal to the stress limit value. In most cases, yield strength corresponds to the stress limit value. A stress limit is a stress at which the deformation continues to increase without increasing the stress inside the product. Units of measurement of yield strength are N/m^2 . Thus, the results are shown in the form of equivalent stress diagrams and a graphical representation of color palette directly on the assembly. The location of the maximum internal stress is painted in red and marked with a footnote to the current stress value.

3.1. A spatial model of robot's lower leg

During the simulation process, assemblies were exposed to 2 types of loads - torque and linear force aimed at three directions: vertical (perpendicular to the transverse plane), lateral (along the normal to the front plane) and lateral (perpendicular to the sagittal plane). To study the lower leg model, we have conducted four experiments described below:

1) Vertical load of 25 N is applied to the lower leg assembly and is distributed evenly throughout the whole volume of plates of the lower leg. The maximum internal stress of the assembly is concentrated in the plates of the lower leg (Fig. 3 a); the stress value is $4.53 \times 10^5 N/m^2$.

2) The torque of the engine flange (6 N·m) and lateral load of 25 N are applied to the lower leg assembly (Fig. 3 b). The load is almost equally distributed over the entire surface of the lower leg plates. The maximum internal stress of the assembly is found in the stiffening rib (in the attachment

point of a stiffening rib and a lower leg plate); the stress value is 3.79×10^7 N/m². The maximum internal stress of the lower leg plate is in the working hole of a stiffening rib and equals 2.29×10^7 N/m².

3) Load of 20 H is applied to the lower leg assembly (perpendicular to the sagittal plane). The maximum internal stress of the assembly is located in the stiffening rib (Fig. 3) and equals 6.72×10^7 N/m². The maximum internal stress of the lower leg plate is in the working hole of attachment of the stiffening rib and equals 2.45×10^7 N/m².

4) The torque equal to 0,825 N·m, acting along the axis that passes through the center of the transverse plate, is applied to the lower leg assembly. The maximum internal stress of the assembly is on the plate that connects plates of the lower leg (Fig. 3 g); the stress value is $6.13 \cdot 10^5 \cdot$ N/m².

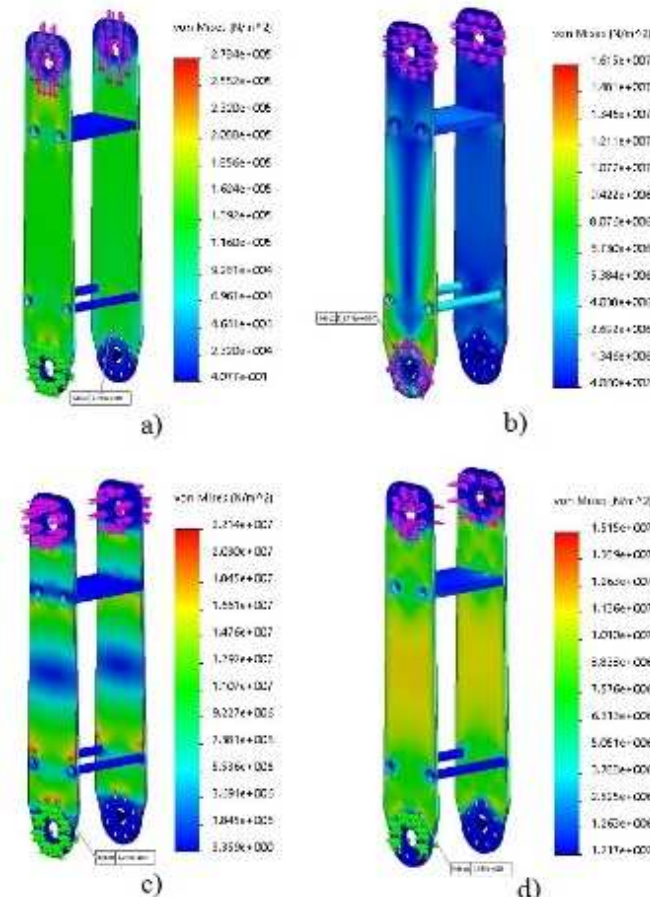


Figure 4. The simulation results of the upper leg model: a) vertical load; b) lateral load (along the normal to the front plane); c) lateral load (perpendicular to the sagittal plane); d) torsion

3.2. A spatial model of robot's upper leg

To study the upper leg model, we have also conducted four experiments described below:

1) Vertical load of 20 N is applied to the upper leg assembly and is evenly distributed throughout the whole volume of plates of the upper leg. The maximum internal stress of the assembly is concentrated in the plates of the upper leg (Fig. 4 a); the stress value is $2.78 \cdot 10^5$ N/m².

2) The torque of the engine flange (6 N·m) and lateral load of 20 N (perpendicular to the transverse plane) are applied to the upper leg assembly. The load is evenly distributed over the entire surface of the upper leg plates. The maximum internal stress of the assembly is on the plates of the upper leg (Fig. 4 b) and equals $1.61 \cdot 10^7$ N/m².

3) Load of 15 H is applied to the upper leg assembly (perpendicular to the sagittal plane). The maximum internal stress of the assembly is on the plates of the upper leg (Fig. 4 b) and equals $2.21 \cdot 10^7$ N/m².

4) The torque, equal to 0.825 N·m, acting along the axis that passes through the center of the transverse plate is applied to the upper leg assembly. The maximum internal stress of the assembly is on the plates of the upper leg (Fig. 4 d); the stress value is $6.13 \cdot 10^5$ N/m².

On the basis of the yield strength for the developed leg model, it can be concluded that the assembly of the upper and lower leg can withstand the given types of external loads, since the yield strength for the leg assembly lies within the permissible range [12, 15].

4. Conclusion

In this paper, we have presented motion analysis of lower limbs of robot Antares, and, on the basis of the obtained results, we have simulated application of external loads on the composite parts of robot's legs. According to the data presented in Figures 3 and 4, it can be concluded that by applying various external forces to the legs, the internal stress is close to the yield point for the given material.

Since the assemblies of robot's structure can withstand the load, calculated previously, without being destroyed, the stability of the leg's design is kept. During the simulation process, we have also identified some of the parameters of the future robot model. The lifting of the robot from the "sitting" position requires torque which is 2.4 times less than the maximum torque developed by the engine, and the construction of the leg can withstand the maximum torque. Thus, the robot is able to perform a vertical jump, which has been successfully confirmed experimentally.

The robot under development is intended for use for educational purposes, such as participation in robot football competitions, as well as for the development of assistive technologies of human-computer interaction based on multimodal interfaces [17-22].

5. Acknowledgments

This work is partially supported by state research 0073-2015-0005 and RSF (grant No. 16-19-00044).

References

- [1] Gradeckij V G, Ermolov I L, Knjaz'kov M M, Semenov E A, Suhanov A N 2014 Kinematicheskaja model' jekzoskeleta ruki cheloveka i opredelenie oshibki pozicionirovanija *Mehatronika, Avtomatizacija, upravlenie. Teoreticheskij i prikladnoj nauchno-tehnicheskij zhurnal.* **5** 37-41
- [2] Zhidenko I G , Kutlubaev I M 2014 *Metodika opredelenija signalov upravlenija antropomorfnyh robotom Mehatronika, Avtomatizacija, upravlenie. Teoreticheskij i prikladnoj nauchno-tehnicheskij zhurnal.* **5** 41-46
- [3] Filatov V V 2014 Ispol'zovanie SAPR Solid Works Motion dlja issledovanija plavnosti hoda transportnogo sredstva. *Transportnaja tehnika, jelektronnyj nauchnyj zhurnal.* **1** 1-7
- [4] Sagirov Ju G 2013 Prochnostnoj analiz metallokonstrukcii gruzopod-emnyh kranov s ispol'zovaniem Solid Works. *Vestnik Priezovskogo gosudarstvennogo tehničeskogo universiteta. Serija: Tehničeskie nauki.* **26** 194-203
- [5] Warnakulasooriyaa S., Bagheria A., Sherburnb N., Shanmugavel M. 2012 Bipedal walking robot – a developmental design *Procedia Eng.* **41** 1016–1021
- [6] Lima S.C., Yeapa G.H. 2012 The locomotion of bipedal walking robot with six degree of freedom *Procedia Eng.* **41** 8–14
- [7] Yoo J.K., Lee B.J., Kim J.H. 2009 Recent progress and development of the humanoid robot. *Hansaram. Rob. Auton. Syst.* **57** 973–981
- [8] Buschmann T., Lohmeier S., Ulbrich H. 2009 Humanoid robot Lola: design and walking control. *J. Physiol.* **103** 141–148
- [9] Mohameda Z., Capi G. 2012 Development of a new mobile humanoid robot for assisting elderly people. *Procedia Eng.* **41** 345–351
- [10] Nakashima M., Tsunoda Y. 2015 Improvement of crawl stroke for the swimming humanoid robot to establish an experimental platform for swimming research. *Procedia Eng.* **112** 517–521
- [11] Poppy [Jelektronnyj resurs] <https://www.poppy-project.org/> (Data obrashhenija 25.08.16)
- [12] DARwin OP [Jelektronnyj resurs] <http://www.robotis.com/> (Data obrashhenija 25.08.16)
- [13] Koval'chuk A K, Kulakov D B, Semenov S E, Jaroc V V, Verejkin A A, Kulakov B B,

- Karginov L A 2014 Metod proektirovanija prostranstvennyh drevovidnyh ispolnitel'nyh mehanizmov shagajushhijh robotov *Inzhenernyj vestnik: jelektronnyj nauchno-tehnicheskij zhurnal* **11** 6-10
- [14] Verejkin A A, Koval'chuk A K, Kulakov D B, Semenov S E 2014 Analiz i vybor kinematicheskoy struktury ispolnitel'nogo mehanizma jekzoskeleta *Nauka i obrazovanie: jelektronnoe nauchno-tehnicheskoe izdanie* **7** 72-93
- [15] Seliverstov G V 2013 Opredelenie koncepcii naprjazhenij pri pettinge kranovyh metallokonstrukcij *Izvestija Tul'skogo gosudarstvennogo universiteta. Tehnicheskie nauki. №7-1* 221-225
- [16] Verejkin A A, Koval'chuk A K, Karginov L A 2014 Issledovanie dinamiki ispolnitel'nogo mehanizma jekzoskeleta nizhnih konechnostej s uchjotom reakcij opornoj poverhnosti *Nauka i Obrazovanie. MGTU im. N.Je. Baumana* **12** 256-278
- [17] Pavluk N, Ivin A, Budkov V, Kodyakov A, Ronzhin A. 2016 Mechanical Leg Design of the Anthropomorphic Robot Antares International conference on interactive collaborative robotics. *ICR 2016* (Springer, LNAI 9812) 113–123
- [18] Karpov A A, Ronzhin A L. 2009 Information Enquiry Kiosk with Multimodal User Interface *Pattern Recognition and Image Analysis, Moscow: MAIK Nauka/Interperiodica* **19** (3) 546-558
- [19] Karpov A, Ronzhin A, Kipyatkova I. 2011 An Assistive Bi-modal User Interface Integrating Multi-channel Speech Recognition and Computer Vision. *In Proc. 14th International Conference on Human-Computer Interaction HCII 2011*, Springer-Verlag Berlin Heidelberg, LNCS 6762, Orlando, FL, USA. 454-463
- [20] Motienko A I, Tarasov A G, Dorozhko I V, Basov O O 2016 Proactive control of Robotic Systems for Rescue Operations. *SPIIRAS Proceedings* **46** 169-189
- [21] Yusupov R M, Ronzhin A L, Prishchepa M V, Ronzhin, Al L. 2011 Models and hardware-software solutions for automatic control of intelligent hall. *Automation and Remote Control.* **72** (7) 1389-1397
- [22] Kryuchkov B I, Karpov A A, Usov V M 2014 Promising Approaches for the Use of Service Robots in the Domain of Manned Space Exploration. *SPIIRAS Proceedings* **32** 125-151